Investigation of the magnetic properties and exchange interactions in gadolinium orthochromite

D. V. Belov, N. P. Kolmakova, I. B. Krynetskiĭ, V. N. Milov, A. A. Mukhin, and V. A. Semenov

Institute of General Physics, Academy of Sciences of the USSR; M. V. Lomonosov State University, Moscow

The magnetic properties of $GdCrO_3$ are studied for a wide range of magnetic fields and temperatures $T_{N2} < T < T_{N1}$ with allowance for the Cr–Cr, Gd–Cr, and Gd–Gd interactions. The angular momenta and threshold field strengths $H_{thr}^a(T)$ are measured and compared with the theoretical values in order to deduce all the parameters characterizing the magnetic interactions in $GdCrO_3$. In particular, the parameters of the isotropic and anisotropic parts of the Gd–Cr interaction Hamiltonian, which are important in determining the magnetic properties of $GcCrO_3$, are found.

1. INTRODUCTION

This paper is concerned with an experimental and theoretical analysis of the magnetic (exchange) interactions in gadolinium orthochromite $GdCrO_3$, which is a weak ferromagnetic material with rhombic symmetry. Gadolinium orthochromite is of interest primarily because of the role of anisotropic Gd–Cr exchange in determining its magnetic properties. Since the Gd^{3+} ion is in the S-state and the orbital momentum of the Cr^{3+} ion is "frozen," the theory predicts[1-5] that isotropic (Heisenberg) exchange should give the dominant contribution to the Hamiltonian describing their hyperfine exchange interaction. On the other hand, some of the magnetic properties of $GdCrO_3$ (e.g., the spontaneous spin-flip transition $\Gamma_4(G_x F_z) \mapsto \Gamma_2(F_z F_x)$ at $T_R = 6.5$ K (Ref. 6) as the temperature is decreased) indicate that the anisotropic Gd–Cr interaction— and in particular,[6,7] the antisymmetric Gd–Cr exchange[1]—play an appreciable role. However, the parameters of the anisotropic Gd–Cr interaction cannot be found explicitly solely on the basis of existing data for $GdCrO_3$ (the magnetization curves,[6] the temperature dependence $m_{a,c}(T)$ of the spontaneous weak ferromagnetic moments along the a and c axes,[7] etc.[8,10]). In order to do this, one must develop an adequate model for $GdCrO_3$ which is capable of describing its magnetic properties in a wide range of temperatures and magnetic fields.

Some of the parameters for the Cr–Cr, Gd–Cr, and Gd–Gd interactions were calculated numerically in Ref. 10 by comparing the theoretical and experimental values for the weak ferromagnetic moments $m_{a,c}(T)$. However, the experimental data were too scanty to permit the determination of several important parameters of $GdCrO_3$.

Our purpose in this work is to find all of the Cr–Cr, Gd–Cr, and Gd–Gd interaction parameters responsible for determining the behavior of the system for $T > T_{N2} = 2.3$–2.4 K, where T_{N2} is the antiferromagnetic transition point for the Gd^{3+} ions.[6,7] We deduce these parameters numerically from angular momentum curves which we recorded for a wide range of temperatures and magnetic fields, and from the H_{thr}^a–T phase diagram for the threshold fields. These experimental data yield much information concerning $GdCrO_3$, including the coefficients of the thermodynamic potential for $GdCrO_3$ and, in particular, the parameters of the Gd–Cr exchange interactions. We were also able to separate the isotropic and anisotropic contributions.

2. EXPERIMENT

We found the magnetic interaction parameters for $GdCrO_3$ by recording the angular momentum and magnetostriction curves during a field-induced $\Gamma_{42} \to \Gamma_2$ spin-flip transition. These curves were then used to deduce the H_{thr}^a–T phase diagram.

The cubic $3 \times 3 \times 3$ mm³ $GdCrO_3$ sample was cut from a single crystal grown by spontaneous crystallization from a solution in a melt. The sides of the cube coincided with the a, b, and c axes of the rhombic crystal to within 2°. We used a strain-gage torque magnetometer to record the angular momentum curves $(L_{rot}^y(\theta_H) \equiv L_{rot}(\theta_H))$ in the ac plane for $2 \leqslant T \leqslant T_{N1} = 170$ K and magnetic fields $\leqslant 10$ kOe. The sample temperature was held constant to within 0.1 K and the magnetometer sensitivity was 15 dyn·cm.

The solid curves in Fig. 1 show some typical measurements. We see that the behavior of the curves depends on T and H: they are continuous for $H > H_{thr}^a(T)$ (Fig. 1a, b) but have discontinuities (jumps) at $\theta_H = \pm \pi/2$ for $H < H_{thr}^a(T)$ (Fig. 1b, c). We also note that the $L_{rot}(\theta_H)$ curves become negative for T below the phase transition point (Fig. 1a).

We used a quartz piezoelectric transducer bonded to the ac-face of the crystal along the c-axis to measure the magnetostriction for temperatures $4.2 \leqslant T \leqslant 170$ K and pulsed magnetic fields H up to 140 kOe parallel to the a axis. The sensitivity was better than $1 \cdot 10^{-7}$, which corresponded to an absolute sample deformation of $\Delta l = 1 \cdot 10^{-10}$ m. The relative error in each series of magnetostriction measurements was less than $\Delta \lambda_c / \lambda_c = \pm 5\%$. Because of calibration errors, the error in the absolute values was as large as $\pm 20\%$.

We deduced the threshold field $H_{thr}^a(T)$ from the field dependence $\lambda_c(H^a)$ of the magnetostriction, which had a
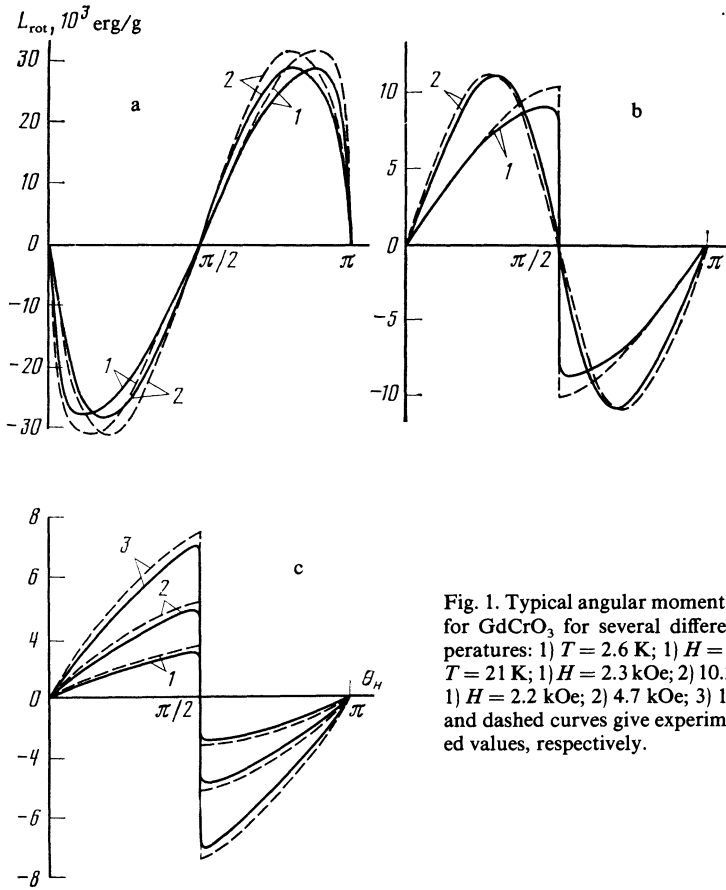
Fig. 1. Typical angular momentum curves $L_{rot}(\theta_H)$ for $GdCrO_3$ for several different fields and temperatures: 1) $T = 2.6$ K; 1) $H = 2$ kOe; 2) 4 kOe; b) $T = 21$ K; 1) $H = 2.3$ kOe; 2) 10.2 kOe; c) $T = 65$ K; 1) $H = 2.2$ kOe; 2) 4.7 kOe; 3) 10.3 kOe. The solid and dashed curves give experimental and calculated values, respectively.

characteristic breakpoint at the field H^a corresponding to the induced $\Gamma_{42} \rightarrow \Gamma_2$ spin-flip transition. Some typical $\lambda_c(H^a)$ curves are shown in the insert to Fig. 2; the maximum error in determining H^a_{thr} was $\sim 10\%$. Figure 2 shows the $H^a_{thr}-T$ diagram found by this method. We will discuss and analyze the observed dependences $H^a_{thr}(T)$ and $L_{rot}(\theta_H,H,T)$ in the next section.

3. THEORY AND ANALYSIS OF THE EXPERIMENTAL DATA

1. The thermodynamic potential

The isotropic Cr–Cr exchange is the strongest interaction in $GdCrO_3$; it is considerably stronger than the Gd–Cr and Gd–Gd interactions and determines the Néel point $(T_{N1} = 170$ K) and the magnetic moments $M_{1,2}$ of the Cr subsystem. We can therefore write the $GdCrO_3$ potential as the sum $\Phi = \Phi_{Cr} + \Phi_{Gd}$ (Ref. 11), where the potential Φ_{Cr} of the Cr subsystem is determined solely by the Cr–Cr interaction and Φ_{Gd}, the potential of the Gd subsystem, is determined by the Gd–Cr and Gd–Gd interactions.

We will use the expression[12]

$$\Phi_{Cr}(\mathbf{F}, \mathbf{G}) = \tfrac{1}{2}A\mathbf{F}^2 + \tfrac{1}{2}D(\mathbf{FG})^2$$
$$+ \tfrac{1}{2}\sum b_i G_i^2 + d(F_z G_x - F_x G_z) - M_0 \mathbf{FH} \qquad (1)$$

for Φ_{Cr}, where $\mathbf{F} = (\mathbf{M}_1 + \mathbf{M}_2)/2M_0$, $\mathbf{G} = (\mathbf{M}_1 - \mathbf{M}_2)/2M_0$ are the ferro- and antiferromagnetic vectors for the Cr subsystem; $M_0 = M_{1,2}(T = 0)$.

Expression (1) is valid for $F \ll G$. The temperature dependences $|\mathbf{G}| = G_0(T), D(T)$, and $b_i(T)$ are specified in (1) either phenomenologically or on theoretical grounds, e.g., by using
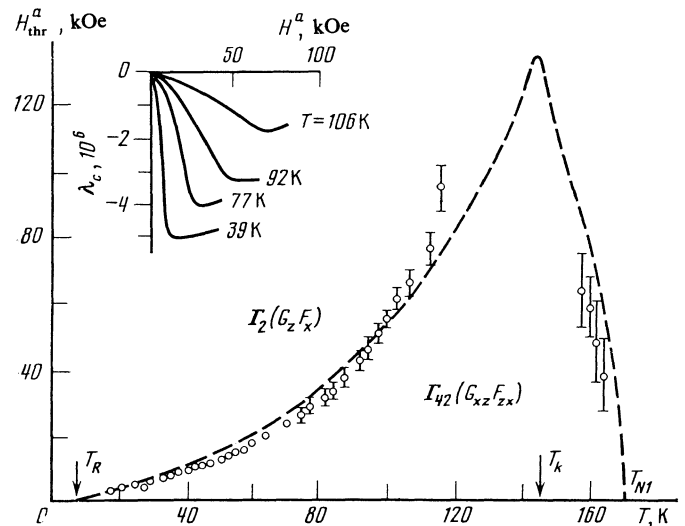

Fig. 2. Temperature dependence of the threshold field $H^a_{thr}(T)$ for the $\Gamma_{42} \rightarrow \Gamma_2$ transition in $GdCrO_3$. The points and the dashed curve show the experimental and calculated values, respectively. The insert shows some typical experimental magnetostriction curves $\lambda_c(H^a)$ from which the threshold field H^a_{thr} was determined.

625   Sov. Phys. JETP 61 (3), March 1985

Belov et al.   625

the molecular field approximation, cf. below.

We now consider the potential of the Gd subsystem. Since the crystal field does not appreciably split the ground state of the Gd^{3+} ion, the dominant interaction is with the external magnetic field $\mathbf{H}$ and the effective field produced by the Cr subsystem. This interaction can be described by the Hamiltonian

$$\mathscr{H}_{Gd}^{\pm} = -g_J\mu_B\mathbf{J}_{Gd}(\mathbf{H}+a\mathbf{F}+\hat{P}^{\pm}\mathbf{G}) \equiv -g_J\mu_B\mathbf{J}_{Gd}\mathbf{H}_{eff}^{\pm}, \qquad (2)$$

where $\mathbf{J}_{Gd}$ is the total momentum operator of Gd^{3+}, $g_J = 2$, a is the Gd–Cr isotropic exchange constant, and the matrix[13]

$$\hat{P}^{\pm} = \begin{pmatrix} 0 & 0 & p_{xz} \\ 0 & 0 & \pm p_{yz} \\ p_{zx} & \pm p_{zy} & 0 \end{pmatrix} \qquad (3)$$

for the anisotropic Gd–Cr exchange includes both the dipole interaction and the anisotropic Gd–Cr exchange. The $\pm$ signs correspond to the two crystallographically inequivalent positions of the Gd^{3+} ions.

The Gd subsystem is paramagnetic for the temperatures $T > T_{N2}$ of interest, and its magnetic moments $\mathbf{m}_G^{(12)}$ are determined by the effective fields $\mathbf{H}_{eff}^{\pm}$:

$$\mathbf{f}_{Gd} = (\mathbf{m}_{Gd}^{(1)}+\mathbf{m}_{Gd}^{(2)})/2 = \chi_R(\mathbf{H}_{eff}^{+}+\mathbf{H}_{eff}^{-})/2,$$
$$\mathbf{c}_{Gd} = (\mathbf{m}_{Gd}^{(1)}-\mathbf{m}_{Gd}^{(2)})/2 = \chi_R'(\mathbf{H}_{eff}^{+}-\mathbf{H}_{eff}^{-})/2, \qquad (4)$$

where

$$\chi_R = C/(T+\Theta), \quad \chi_R' = C/(T+\Theta'), \quad C = Ng_J^2\mu_B^2 J_{Gd}(J_{Gd}+1)3k_B$$

are the isotropic paramagnetic susceptibilities of the Gd subsystem and determine how the latter responds to the effective fields, which induce ferromagnetic ($\mathbf{f}_{Gd}$) and antiferromagnetic polarizations ($\mathbf{c}_{Gd}$). Here χ_R and χ_R' differ slightly due to differences in the Gd–Gd interaction for the $\mathbf{f}_{Gd}$ and $\mathbf{c}_{Gd}$ polarizations; we allow for this difference by using the two Curie temperatures Θ and Θ'. For $m_{Gd}{}^0 H_{eff} \ll k_B T$ we thus obtain

$$\Phi_{Gd}(\mathbf{F,G}) = -\frac{1}{2}\chi_R\left(\frac{\mathbf{H}_{eff}^{+}+\mathbf{H}_{eff}^{-}}{2}\right)^2 - \frac{1}{2}\chi_R'\left(\frac{\mathbf{H}_{eff}^{+}-\mathbf{H}_{eff}^{-}}{2}\right)^2. \qquad (5)$$

The complete thermodynamic potential of the system is given by

$$\Phi(\mathbf{F,G}) = {}^1/_2\tilde{A}\mathbf{F}^2+{}^1/_2 D(\mathbf{FG})^2+{}^1/_2\sum\tilde{b}_i G_i^2 - \tilde{d}_1 F_x G_z \\ -\tilde{d}_3 F_z G_x - (1+\eta)M_0\mathbf{FH} - \tau_1 H_x G_z - \tau_3 H_z G_x - {}^1/_2\chi_R H^2, \qquad (6)$$

where

$$\tilde{b}_1 = b_1 - \chi_R p_{zx}^2, \quad \tilde{b}_2 = b_2 - \chi_R' p_{zy}^2,$$
$$\tilde{b}_3 = b_3 - \chi_R p_{xz}^2 - \chi_R' p_{yz}^2, \quad \tau_1 = \chi_R p_{xz}, \quad \tau_3 = \chi_R p_{zx}, \quad \eta = a\chi_R/M_0,$$
$$\tilde{d}_1 = d+a\tau_1, \quad \tilde{d}_3 = -d+a\tau_3, \quad \tilde{A} = A-\chi_R a^2. \qquad (7)$$

We now minimize (6) with respect to $\mathbf{F}$, eliminate $\mathbf{F}$, and express Φ in terms of the unit vector $\mathbf{v} = \mathbf{G}/|\mathbf{G}|$:

$$\Phi(\mathbf{v}) = {}^1/_2 K_{ac}v_z^2+{}^1/_2 K_{ab}v_y^2+{}^1/_4 K_2 v^4+{}^1/_4 K_2'v_y^4 \\ +{}^1/_2 K_2''v_z^2 v_y^2 - m_x H_x v_z - m_z H_z v_x - m'v_x v_z(\mathbf{Hv})$$

$$-{}^1/_2(\chi_{\perp}+\chi_R)\mathbf{H}^2+{}^1/_2\Delta\chi(\mathbf{Hv})^2, \qquad (8)$$

where

$$K_{ac} = [K_{ac}{}^{Cr}-\chi_R'p_{yz}^2-\tilde{\chi}_R(H_{eff}^{x2}-H_{eff}^{z2})+\Delta K_{Gd}]G_0^2,$$

$$\Delta K_{Gd} = \eta\xi\tilde{\chi}_R(H_{eff}^x+H_{eff}^z)^2,$$

$$K_{ab} = [K_{ab}{}^{Cr}-\chi_R'p_{zy}^2+\tilde{\chi}_R H_{eff}^{z2}]G_0^2,$$

$$K_{ac}{}^{Cr} = b_3 - b_1, \quad K_{ab}{}^{Cr} = b_2 - b_1,$$

$$K_2 = K_2{}^{Cr}-2\Delta K_{Gd}G_0^2, \quad K_2' = K_2'{}^{Cr}, \quad K_2'' = K_2''{}^{Cr}-\Delta K_{Gd}G_0^2,$$

$$m_x = (m_{Cr}{}^0+\tilde{\chi}_R H_{eff}^x)G_0, \quad m_z = (-m_{Cr}{}^0+\tilde{\chi}_R H_{eff}^z)G_0, \qquad (9)$$

$$m_{Cr}{}^0 = M_0 d/A,$$

$$H_{eff}^x = p_{xz}+ad/A, \quad H_{eff}^z = p_{zx}-ad/A,$$

$$m' = -\xi(1+\eta)\tilde{\chi}_R(H_{eff}^x+H_{eff}^z)G_0,$$

$$\xi = \varkappa\Delta\chi^{Cr}/(1-\varepsilon_{\|}), \quad \varkappa = a/M_0, \quad \chi_{\perp} = \chi_{\perp}{}^{Cr}(1+\eta)^2/(1-\varepsilon_{\perp}),$$
$$\Delta\chi = \Delta\chi^{Cr}(1+\eta)^2/(1-\varepsilon_{\perp})(1-\varepsilon_{\|}), \quad \Delta\chi^{Cr} = \chi_{\perp}{}^{Cr}-\chi_{\|}{}^{Cr},$$
$$\varepsilon_{\perp,\|} = \varkappa^2\chi_R\chi_{\perp,\|}{}^{Cr}, \quad \chi_{\perp}{}^{Cr} = M_0^2/A \equiv M_0/2H_E,$$
$$\tilde{\chi}_R = \chi_R/(1-\varepsilon_{\perp}) = C/(T+\tilde{\Theta}), \quad \tilde{\Theta} = \Theta - C\varkappa^2\chi_{\perp}{}^{Cr}.$$

We will use the molecular field approximation for the temperature dependences $\chi_{\|}^{Cr}(T)$ and $G_0(T)$, which are important for $T \approx T_{N1}$. This approximation gives

$$\chi_{\|}{}^{Cr}(T) = \chi_{\perp}{}^{Cr}(1+\Delta(T))^{-1}, \qquad (10)$$

where

$$\Delta(T) = \frac{Nk_B T_{N1}\chi_{\perp}{}^{Cr}}{M_0^2}\left[\frac{T}{T_{N1}B_{3/2}'}-\frac{3S_{Cr}}{S_{Cr}+1}\right], \qquad (11)$$

and $G_0(T)$ can be calculated from the equation

$$G_0 = B_{3/2}(x), \quad x = 3S_{Cr}G_0 T_{N1}/T(S_{Cr}+1), \qquad (12)$$

where $B_{3/2}$ is the Brillouin function.[2] We note that since $S_{Cr} = 3/2$, the crystal field does not contribute to the fourth-order anisotropy constants of the Cr subsystem. The contribution ΔK_{Gd} from the Gd–Gd interaction to K_2 and K_2' is proportional to the small parameter $\xi \sim a/2H_E$ and will be neglected, along with the contribution from the Cr subsystem to the magnetostriction; we will set K_2, K_2', and K_2'' equal to zero.[3]

The above fundamental expression for the potential Φ can be used to calculate all the observable magnetic properties of $GdCrO_3$ for $T_{N2} < T < T_{N1}$. The strong dependence of the coefficients on the temperature and the Cr–Cr, Gd–Cr, and Gd–Gd interaction parameters makes it possible to deduce them by comparing the calculated characteristics with the experimental results.

In what follows we will first use (8) to qualitatively analyze the observable magnetic properties of $GdCrO_3$; we will then discuss the numerically calculated parameters.

2. Spontaneous and induced spin-flip transitions in GdCrO₃

Expression (9) for K_{ac} shows that the anisotropic Gd–

Cr interaction will give a negative contribution to the effective anisotropy constant in the ac plane which increases as T decreases. This contribution is the reason for the $\Gamma_4 \rightarrow \Gamma_2$ spin reorientation which is observed in GdCrO$_3$ at $T_R \approx 6.5$ K (Ref. 6). The temperature T_R is defined by the condition $K_{ac}(T_r) = 0$ and is equal to

$$T_R \approx [\,(T_1+T_2)^2 + 2(T_1-T_2)(\Theta'-\widetilde{\Theta}) + (\Theta'-\widetilde{\Theta})^2]^{1/2} - (\Theta'+\widetilde{\Theta})/2, \tag{13}$$

where

$$T_1 = C(H_{\text{eff}}^{x^2} - H_{\text{eff}}^{z^2})/K_{ac}{}^{\text{Cr}}, \qquad T_2 = Cp_{yz}{}^2/K_{ac}{}^{\text{Cr}}.$$

The weak ferromagnetic moments $m_c(T)$ in the Γ_4 GdCrO$_3$ phase and $m_a(T)$ in the Γ_2 phase are given by the expressions

$$m_c(T) = m_z(T)v_x{}^0 = m_{\text{Cr}}{}^c + \widetilde{\chi}_R H_{\text{eff}}{}^c G_0, \tag{14}$$

where

$$m_{\text{Cr}}{}^c = -m_{\text{Cr}}{}^0 G_0 v_z{}^0, \qquad H_{\text{eff}}{}^c = H_{\text{eff}}{}^z v_x{}^0, \qquad v_x{}^0 = \pm 1,$$

$$m_a(T) = m_x(T)v_z{}^0 = m_{\text{Cr}}{}^a + \widetilde{\chi}_R H_{\text{eff}}{}^a G_0, \tag{15}$$

$$m_{\text{Cr}}{}^a = m_{\text{Cr}}{}^0 G_0 v_z{}^0, \qquad H_{\text{eff}}{}^a = H_{\text{eff}}{}^x v_z{}^0, \qquad v_z{}^0 = \pm 1.$$

We note that unlike $m_{x,z}$ and $H_{\text{eff}}^{x,z}$, $m_{a,c}$ and $H_{\text{eff}}^{a,c}$ are of constant sign in the Γ_4 (or Γ_2) equilibrium states. Experimental results[6,7] indicate that the weak ferromagnetic moment $m_c(T)$ along the c axis vanishes at a temperature $T = T_k^c$ whose value appears to vary somewhat ($T_k^c = 143$ K in Ref. 7 and 110 K in Ref. 6). Analysis of the experimental data in Ref. 6 indicates that $m_a(T)$ also vanishes at a point $T_k^a \approx T_k^c$. This implies that the effective fields H_{eff}^a and H_{eff}^c are both of negative sign. We also note that H_{eff}^x and H_{eff}^z have opposite signs:

$$H_{\text{eff}}^x = H_{\text{eff}}^a v_z{}^0 = H_{\text{eff}}^a \operatorname{sign} d, \qquad H_{\text{eff}}^z = H_{\text{eff}}^c v_x{}^0 = -H_{\text{eff}}^c \operatorname{sign} d.$$

According to Ref. 6, $H_{\text{eff}}^a = -6.4 \pm 0.5$ kOe and $H_{\text{eff}}^c = -5.5 \pm 0.2$ kOe.

The systems is in the Γ_4 phase for $T > T_R$, and a spin-flip transition to the Γ_2 phase occurs when an external magnetic field **H** is applied parallel to the a axis. The threshold field $H_{\text{thr}}^a(T)$ for the $\Gamma_{42} \rightarrow \Gamma_2$ transition is determined by $(\partial^2\Phi/\partial\theta^2)_{\theta=0,\pi} = 0$ and is given by

$$H_{\text{thr}}^a(T) = \frac{|m_x - 2m'|}{2\Delta\chi}\left[\left(1 + \frac{4K_{ac}\Delta\chi}{|m_x-2m'|^2}\right)^{1/2} - 1\right]. \tag{16}$$

This formula accurately reflects the qualitative and quantitative behavior of the observed dependence $H_{\text{thr}}^a(T)$ (cf. below). We have $H_{\text{thr}}^a \approx K_{ac}/|m_x - 2m'| \rightarrow 0$ for $T \rightarrow T_R$ or T_{N1}, while H_{thr}^a has a maximum $\sim (K_{ac}/\Delta\chi)^{1/2}$ for $T \sim T_k^a$ (Fig. 2). For $T < T_R$, an external magnetic field **H** parallel to the c axis will similarly induce a $\Gamma_2 \rightarrow \Gamma_4$ phase transition. The threshold field in this case is given by (16) with m_x and K_{ac} replaced by m_z and $-K_{ac}$, respectively.

3. Behavior of the angular momentum in the ac-plane

When the external field rotates in the ac plane, an angular momentum acts on the crystal along the b (y) axis:

$$L_{\text{rot}}{}^y \equiv L_{\text{rot}} = [\mathbf{H}, \partial\Phi/\partial\mathbf{H}]_y = \partial\Phi/\partial\theta_H.$$

Here the equilibrium values of **v** are found from the equation $\partial\Phi/\partial\theta = 0$, where the angles θ and θ_H determine the orientation of **v** (or **G**) and **H** relative to the c axis in the ac plane. It is not possible to derive exact analytic expressions for L_{rot} for arbitrary orientations of **H**; we will therefore analyze L_{rot} by using approximate formulas valid for certain magnetic field ranges.

1) For weak fields ($H \ll H_{\text{thr}}^a$),

$$L_{\text{rot}} \approx v_x{}^0 m_z H \sin\theta_H[1 - (\chi_{\text{rot}} H^2/K_{ac})f(\theta_H)] + {}^1/_2(\Delta\chi - \chi_{\text{rot}})H^2 \sin 2\theta_H, \tag{17}$$

where

$$\chi_{\text{rot}} = (m_x + m')^2/K_{ac}, \qquad v_x{}^0 = \operatorname{sign}(m_z \cos\theta_H),$$

and the function $f(\theta_H)$ is ~ 1. When θ_H passes through the values $\pm\pi/2$, i.e., when the sign of the projection of **H** on the c axis changes, the system goes from one angular phase into the other (for $H < H_{\text{thr}}^a$) and there is an abrupt jump ("discontinuity") in the curve $L_{\text{rot}}(\theta_H)$ which is described by the first term in Eq. (17). The magnitude of the jump initially increases with H but then decreases and vanishes for $H = H_{\text{thr}}^a$. Figure 1b, c shows some typical experimental curves $L_{\text{rot}}(\theta_H)$ for GdCrO$_3$ in this case.

b) For strong fields ($\Delta\chi H^2 \gg K_{ac}, |m_{x,z}|H$),

$$L_{\text{rot}} = \sin 2\theta_H[{}^1/_2 K_{ac} + H(m_x + m_z)\operatorname{sign} m_z]. \tag{18}$$

In this case the angular dependences $L_{\text{rot}}(\theta_H)$ are smooth curves without any jumps (Fig. 1a, b).

We note that Eq. (18) in fact remains valid for GdCrO$_3$ for a wider range of fields: $H \gg |K_{ac}/m_{x,z}|$. This is a consequence of the small anisotropies of the weak ferromagnetic moments along the a and c axes $m_x \approx -m_z$ or $H_{\text{eff}}^x \sim -H_{\text{eff}}^z$), as can be seen from the fact that the curves $L_{\text{rot}}(\theta_H)$ are almost independent H for this range of fields (Fig. 1a). The anisotropy constant K_{ac} (18) thus gives the dominant contribution to L_{rot} in this case. This is particularly apparent in the change of sign in the $L_{\text{rot}}(\theta_H)$ curves when T passes through the reorientation transition point $T_R \approx 6.5$ K (Fig. 1a, b).

4. NUMERICAL DETERMINATION OF THE MAGNETIC INTERACTION PARAMETERS FOR GdCrO$_3$

We took the nine quantities $\chi_1^{\text{Cr}}, m_{\text{Cr}}^0, K_{ac}^{\text{Cr}}, H_{\text{eff}}^x, H_{\text{eff}}^z, a, p_{yz}, \theta$, and θ' as the independent parameters which describe the magnetic interactions in GdCrO$_3$ and can be found from the experimental data. The other quantities (the parameters of the thermodynamic potential) were taken to be $T_{N1} = 170$ K, $M_0 = 2S_{\text{Cr}}\mu_B N = 65$ G·cm^3/g, $C = 3.15 \cdot 10^{-2}$ cm^3·K/g. The temperature T_k^c at which $m_c(T)$ vanishes was also assumed to lie in the interval $140 < T_k^c < 145$ K (Ref. 7).

The GdCrO$_3$ parameters were calculated to give the closest agreement between the experimental results and the theoretical angular momentum curves (calculated numerically) and threshold fields H_{thr}^a [cf. (16)]. We did this by minimizing the variance

627   Sov. Phys. JETP **61** (3), March 1985

Belov et al.   627

TABLE I. Magnetic interaction parameters for GdCrO$_3$ found by comparing theory and experiment.

Parameter	Our work	[6]	[10] *
$\chi_\perp^{Cr}$, cm^3/g	$(1.2-1.8)\,10^{-5}$	–	$1.7 \cdot 10^{-5}$
m_{Cr}^0, G·cm^3/g	$1.1-1.3$	1.6 (c-axis) 1.9 (a-axis)	1.1
K_{ac}^{Cr}, erg/g	$(3.7-4.0)\,10^4$	–	–
H_{eff}^a, kOe	$-(5.2-5.8)$	-6.4 ± 0.5	–
H_{eff}^c, kOe	$-(5.2-5.7)$	-5.5 ± 0.5	5.4
a, kOe	$-(115-150)$	–	-145
$\lvert p_{yz} \rvert$, kOe	$3.1-3.9$	–	–
Θ, K	$2.4-3.7$	2.3	–
Θ', K	$1.0-1.7$	–	–

*A different terminology was employed in Ref. 10; the values given here are therefore rescaled to correspond to our terminology.

$$V=\sum_{i=1}^{74}\left[1-\frac{L_{rot}^i(\text{th})}{L_{rot}^i(\exp)}\right]^2+\sum_{i=1}^{18}\left[1-\frac{H_{ni}^a(\text{th})}{H_{ni}^a(\exp)}\right]^2 \quad (19)$$

with respect to the nine independent parameters. The number of experimental values L_{rot}^i was chosen large enough to fully reflect the characteristic features of the field, angular, and temperature dependences of the angular momentum but not so large as to increase the computational time unduly. We used a special code based on the grazing error method to minimize V.

The GdCrO$_3$ parameters found by this method are shown in Table I. We found that the minimum value of V was insensitive to variations of $\pm$ 10–15% in the data points (these variations were comparable to the experimental error).

Figures 1 and 2 show some of the experimental and theoretical curves $L_{rot}(\theta_H,H,T)$ and $H_{thr}^a(T)$, which were calculated for $\chi_\perp^{Cr} = 1.49 \cdot 10^{-5}$ cm^3/g, $m_{Cr}^0 = 1.19$ G·cm^3/g,

TABLE II. The elements of the anisotropic interaction matrix $\hat{P}$.

Parameter, kOe	$d>0$	$d<0$
$p_{xz} = p_{xz}^{dip} + p_{xz}^{ex}$	$-(2.9-3.2)$	$(2.9-3.2)$
p_{xz}^{ex}	$-(2.5-2.8)$	$(3.3-3.6)$
$p_{zx} = p_{zx}^{dip} + p_{zx}^{ex}$	$(2.9-3.2)$	$-(2.9-3.2)$
p_{zx}^{ex}	$(3.3-3.6)$	$-(2.5-2.8)$
$p_s = (p_{xz} + p_{zx})/2$	~ 0	~ 0
$p_{as} = (p_{xz} - p_{zx})/2 \equiv p_{as}^{ex}$	$-(2.9-3.2)$	$(2.9-3.2)$
$p_s^{ex} = p_s - p_s^{dip}$	0.4	0.4
*$p_{yz} = p_{yz}^{dip} + p_{yz}^{ex}$	$(3.1-3.9)$	$-(3.1-3.9)$
*p_{yz}^{ex}	$(1.4-2.2)$	$-(4.8-5.6)$
$p_{xz}^{dip} = p_{zx}^{dip} = p_s^{dip}$	-0.4	-0.4
$p_{yz}^{dip} = p_{zy}^{dip}$	1.7	1.7

*Here the different signs of p_{yz} are unrelated with the sign of d.

$K_{ac}^{Cr} = 4 \cdot 10^4$ erg/g, $H_{eff}^x = -H_{eff}^z = 5.2$ kOe, $a = -115$ kOe, $\lvert p_{yz} \rvert = 3.8$ kOe, $\theta = 2.79$ K, and $\theta' = 1.55$ K. The minimum $V = 2.43$ found for these parameter values corresponds to a mean square error of 15%.

Table I also presents some of the values found in Refs. 6 and 10 for GdCrO$_3$. On the whole, they agree with our results. The values of H_{eff}^x, H_{eff}^z, a, etc., found by this method can be used to calculate the elements of the matrix $\hat{P}$ describing the anisotropic Gd–Cr interaction:

$$p_{xz} = (H_{eff}^x - a\lvert d\rvert/A)\,\text{sign}\,d, \qquad p_{zx} = (-H_{eff}^z + a\lvert d\rvert/A)\,\text{sign}\,d.$$

where sign (d) is the sign of the Dzyaloshinskiǐ constant d. Table II presents values for the elements of the matrix $\hat{P}$ and separates the exchange from the theoretically calculated dipole contribution. We see that the antisymmetric Gd–Cr exchange gives the dominant contribution to the matrix elements p_{xz} and p_{zx}.

5. CONCLUSIONS

We have thus studied the magnetic properties of GdCrO$_3$ experimentally and theoretically for temperatures $T_{N2} < T < T_{N1}$ and derived the thermodynamic potential of the system, which is determined by the properties of the Cr–Cr, Gd–Cr, and Gd–Gd interactions. The interaction parameters were calculated numerically and compared with experimental data on $H_{thr}^a(T)$ and $L_{rot}(\theta_H,H,T)$. Some of these parameter values are in agreement with the results found previously in Refs. 6 and 10 (cf. Table I). In addition, we have calculated some previously unknown parameters of GdCrO$_3$ (p_{yz}, K_{ac}^{Cr}, etc.), which enabled us to distinguish the isotropic and anisotropic contributions of the Gd–Cr interaction to the effective fields H_{eff}^x and H_{eff}^z experienced by the Gd^{3+} ions. We calculated the corresponding parameters of the $\hat{P}$ matrix for the anisotropic Gd–Cr interaction and showed that the matrix elements p_{xz} and p_{zx} are determined primarily by the antisymmetric Gd–Cr exchange, which accounts for roughly 50% of the total contribution to H_{eff}^x and H_{eff}^z. The anisotropic (and particularly the antisymmetric) contribution to the Gd–Cr interaction is thus important in determining the magnetic properties of GdCrO$_3$.

[1] Anisotropic Gd–Fe exchange has also been found to be appreciable in GdFeO$_3$ (Ref. 9).

[2] In our subsequent quantitative analysis of the experimental data and determination of the parameters of the thermodynamic potential, we will use only the experimental data for $T \lesssim 0.7$ T_{N1}, for which the temperature dependences $G_0(T)$ and $\chi_\parallel^{Cr}(T)$ play a minor role compared to the temperature dependence of the coefficients of the thermodynamic potential (this latter dependence is caused by the Gd–Cr interaction). It is therefore legitimate to employ the molecular field approximation. Although this approximation is not quantitatively correct for T close to T_{N1}, it nevertheless correctly describes the qualitative form of the experimental H_{thr}^a curve (cf. Fig. 2).

[3] Unless T is very close to the transition temperature $T_R \sim 6.5$ K for the $\Gamma_4 \to \Gamma_2$ reorientation and one is interested in the nature of this transition, one may neglect these contributions to K_2, as well as the contribu-

tions from terms which are of higher order in the expansion parameter $m^0_{Gd} H_{eff}/k_B T$ for the thermodynamic potential.[8]

[1]J. H. Van Vleck, Phys. Rev. **52**, 1178 (1937).

[2]P. M. Levy, Phys. Rev. A **135**, 155 (1964).

[3]P. M. Levy, Phys. Rev. **147**, 311 (1966).

[4]B. J. Birgenau, J. Appl. Phys. **40**, 1070 (1969).

[5]R. J. Elliott and M. F. Thorpe, J. Appl. Phys. **39**, 802 (1968).

[6]A. H. Cooke, D. M. Martin, and M. R. Wells, J. Phys. C: Solid State Phys. **7**, 3133 (1974).

[7]K. Tsushima, T. Tamaki, and R. Yamaura, in: Proc. Int. Conf. Magnetism, Vol. 5, Nauka, Moscow (1974), p. 270.

[8]A. S. Karnachev, Yu. I. Klechin, N. M. Kovtun, A. S. Moshvin, and E. E. Solov'ev, in: Proc. Fifth Int. Conf. Gyromagnetic Electronics and Electrodynamics (Vilnius, 1980), Vol. 4, Moscow (1980), p. 47; A. S. Karnachev, Yu. I. Klechin, N. M. Kovtun, et al., Zh. Eksp. Teor. Fiz. **85**, 670 (1983) [Sov. Phys. JETP **58**, 390 (1983)].

[9]D. V. Belov, A. K. Zvezdin, A. M. Kadomtseva, et al., Fiz. Tverd. Tela (Leningrad) **23**, 2831 (1981) [Sov. Phys. Solid State **23**, 1654 (1981)].

[10]S. Washimiya and C. Satoko, J. Phys. Soc. Jpn. **45**, 1204 (1978).

[11]A. K. Zvezdin and A. F. Popkov, Fiz. Met. Metalloved. **50**, 242 (1980).

[12]E. A. Turov and V. E. Naĭsh, Fiz. Met. Metalloved. **9**, 10 (1960).

[13]K. P. Belov, A. K. Zvezdin, A. M. Kadomtseva, and R. Z. Levitin, Orientatsionnye Perekhody v Redkozemel'nykh Magnetikakh (Spin Flip Transitions in Rare-Earth Magnets), Nauka, Moscow (1979), p. 320.

[14]D. M. Himmelblau, Applied Nonlinear Programming, McGraw-Hill, New York (1972).

Translated by A. Mason

629   Sov. Phys. JETP **61** (3), March 1985

Belov *et al.*   629